Naphthoquinone-Imidazolyl Derivatives-Based Oxime Esters as Photoinitiators for Blue LED-Induced Free Radical Photopolymerization

Timur Borjigin, Ji Feng, Nicolas Giacoletto, Michael Schmitt, Fabrice Morlet-Savary, Bernadette Graff, Pu Xiao, Malek Nechab, Didier Gigmes, Frédéric Dumur, et al.

Naphthoquinone-Imidazolyl Derivatives-Based Oxime Esters as Photoinitiators for Blue LED-Induced Free Radical Photopolymerization

Timur Borjigin[1,2], Ji Feng[1,2], Nicolas Giacoletto[3], Michael Schmitt[1,2], Fabrice Morlet-Savary[1,2], Bernadette Graff [1,2], Pu Xiao[4*], Malek.Nechab[3], Didier Gigmes[3], Frédéric Dumur[3*], Jacques Lalevée[1,2*]

[1]Université de Haute-Alsace, CNRS, IS2M UMR 7361, F-68100 Mulhouse, France

[2]Université de Strasbourg, F-67000 Strasbourg, France

[3]Aix Marseille Univ, CNRS, ICR UMR 7273, Marseille, F-13397 France

[4]Research School of Chemistry, Australian National University, Canberra, ACT 2601, Australia

Abstract: In this study, we report the successful design and synthesis of nine novel oxime esters based on the naphthoquinone-imidazolyl scaffold and serving as photoinitiators to trigger photopolymerization processes under visible light. In the presence of acrylate monomers and upon irradiation at 405 nm with a LED, these photoinitiators showed remarkable photoinitiating abilities. Newly developed photoinitiators exhibited a multifunctional photoinitiating ability since these structures could act both as Type I photoinitiators or in multicomponent systems, with an improvement of the monomer conversions in the second case. This performance enhancement was notably evidenced in two-component systems comprising the new compounds in combination with either an iodonium salt or an amine. This enhancement of the monomer conversion can be assigned to favorable interactions between the dyes and the different additives, enabling to improve the free radical generation. The underlying chemical mechanisms that govern the radical chemistry during the different photopolymerization processes were explored through a series of systematic experiments. To end, usefulness of these photoinitiators was confirmed by the successful production of 3D objects using the Direct Laser Write method. This suggests promising applications of these photoinitiators in 3D printing technologies.

Keywords: Naphthoquinone-based photoinitiator; Oxime esters; Blue LED; Direct Laser Writing.

1 Introduction

Photoinitiators have been the focus of intense researches as these structures can be used for a variety of applications ranging from lithographic processes, coatings, adhesive applications and 3D printing. Their broad range of application is notably the result of their unique capabilities to cure and polymerize resins and composites under various irradiation conditions (artificial light sources, daylight or sunlight, under low to high light irradiation conditions[1-3]. Technically, photoinitiators can absorb photons and generate reactive species, typically free radicals, that are capable of initiating polymerization reactions. Photoinitiators can be classified into two different categories, namely Type I photoinitiators that can fragment into radicals, and Type II photoinitiators which can generate radicals by hydrogen abstraction[4,5].

Type I photoinitiators also refer to photocleavable structures, which operate according to a process that involves first the absorption of light, thus promoting the molecule in its excited state, more generally in its singlet excited state. Subsequent to photon absorption, an homolytic cleavage of a selected bond can occur, generating radicals. Each fragment possesses an unpaired electron, and these free radicals are then capable of initiating the polymerization of monomers[6-8]. The remarkable advantage of Type I photoinitiators lies in their ability to function independently, meaning they do not require any co-initiators or synergists for their action. Furthermore, they can be designed to possess a broad range of absorption spectra, making these structures versatile photoinitiators that can be used for various applications[9].

On the other hand, Type II photoinitiators, also known as hydrogen abstraction photoinitiators, operate through a somewhat different mechanism. Upon light absorption, the chromophore is promoted in its excited state and instead of fragmenting, it will react in a bimolecular reaction with a co-initiator or a hydrogen donor. The excited Type II photoinitiator can abstract a hydrogen atom from the co-initiator,

generating a radical on the co-initiator and a radical on the photoinitiator [10-12]. Type II photoinitiators offer the advantage of functioning at longer wavelength than Type I photoinitiators, providing a potential path for the development of photoinitiators with enhanced biocompatibility and deeper light penetration [13].

Recently, there has been a shift towards visible light photopolymerization and especially for processes that can be carried out in the near UV-visible range. Interest for visible light photopolymerization is notably supported by the development of new light sources, namely light-emitting diodes (LEDs) that are cheap, long-living, compact and easily available light sources. Compared to ultraviolet (UV) light, blue LEDs offer a series of advantages such as being safer to the human eye, energy-efficient devices, and to exhibit longer lifespan than the traditional light sources [14]. However, the design and synthesis of photoinitiators that respond efficiently to blue light represents a considerable challenge due to the high energy thresholds required to induce the formation of free radicals. Hence, the development of photoinitiators sensitive to blue light and that can be activated under low light intensity (i.e. LEDs) remains the focus of intense research efforts [15-17].

The quest for designing new and efficient photoinitiators has led researchers to explore different classes of organic compounds. Among this wide variety of structures, one class of compound has gained a considerable attention, namely quinone-based compounds and more specifically naphthoquinones [18-20]. Naphthoquinones are aromatic organic compounds possessing two carbonyl groups and these structures have been shown to possess excellent photophysical and photochemical properties, making them suitable candidates for photoinitiation reactions[21]. Additionally, quinones exhibit an excellent thermal and photochemical stability as well as an easy tunability of the optical properties, which are crucial for their prospective usage in material science[22].

Furthermore, incorporation of imidazole ring systems into photoinitiators has been found to enhance their photoinitiating efficiencies. Imidazoles are planar five-membered ring compounds that contain two nitrogen atoms, which, when coupled with

the right functional groups, can display extraordinary photoinitiating properties[23,24]. This is attributed to their π-conjugated systems, which broadens the absorption spectra and improves their light absorption properties by enhancing the molar extinction coefficients [25].

Oxime esters, on the other hand, are well-known for their radical generation abilities and have been widely explored as Type I photoinitiators [26-28]. Structurally, oxime esters are composed of an oxime functional group (R_1R_2C=NOH) linked to an ester moiety (-COOR), which together form a chromophoric system that can effectively absorb light. Upon absorption of light, oxime esters are promoted in the excited state and an homolytic cleavage of the N-O bond can occur. The point of cleavage is typically the nitrogen-oxygen bond, which leads to the generation of two highly reactive radicals: an alkoxy radical and an iminyl radical[29]. The alkoxy radical then initiate the polymerization process by reacting with the double bond of the acrylic monomer, adding itself onto the monomer and then creating another radical that can propagate, resulting in the polymer chain formation [30]. An interesting feature of oxime esters is the rapid initiation of the polymerization process. This high speed is attributed to the relatively low energy required for the homolytic cleavage, which is in turn driven by the instability of the oxime ester bond in the excited state. Presence of the oxime group as a peripheral group also enables to connect this photocleavable group to various chromophores, generating dyes absorbing in the UV/near visible region but also in the visible region, making oxime esters compatible with a variety of light sources, including LEDs[31,32].

The unique combination of properties — rapid initiation, stability, non-yellowing, and potential compatibility with long wavelength light sources — makes oxime esters versatile and powerful agents in photopolymerization. The potential synergy between naphthoquinones, imidazoles, and oxime esters has not been fully investigated yet.

This paper aims at exploring the design, synthesis, and photoinitiating efficiency of naphthoquinone-based imidazolyl oxime esters in free radical photopolymerization experiments. Upon exposure to standard LEDs emitting at 405 nm, this series of

innovative photoinitiators, consisting of nine dyes differing by the ester group introduced on the oxime ester side, were demonstrated to effectively trigger the polymerization of a trifunctional acrylate monomer (TMPTA), both as Type I photoinitiators or in multicomponent systems. The polymerization process, including its rate and outcomes, can be rigorously and comprehensively analyzed through in situ infrared spectroscopy measurements, providing real-time insights. These photoinitiators display significant light absorption properties at 375 nm, a characteristic that endows them with the necessary features for facilitating photochemical reactions within the near-visible spectrum. The underlying photochemical mechanism was thoroughly investigated using a series of complementary techniques. These methods provided a rich array of data that enabled to elucidate the key processes and dynamics involved in the reactions mediated by these photoinitiators. In the final stage of this study, these photoinitiators were utilized in 3D printing, employing a direct laser writing technique. This resulted in the creation of three-dimensional patterns that displayed outstanding resolutions, further illustrating the potential applications of these photoinitiators in practical settings. The unique blend of these three components could offer new insights into the development of next-generation blue-LED-sensitive photoinitiators.

2 Methods and Materials

This study reports the synthesis of nine unreported naphthoquinone-imidazolyl derivatives-based oxime esters (as shown in Scheme 1). The detailed methodology for their synthesis is presented in the Supporting Information (SI) section.

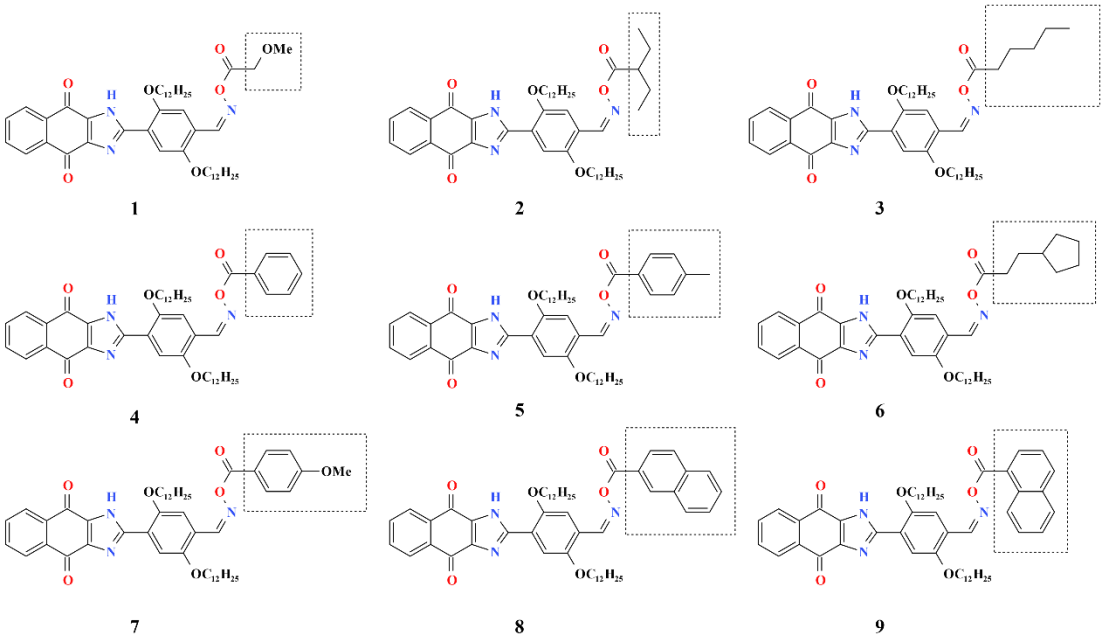

Scheme 1. Chemical structures of naphthoquinone-imidazolyl derivatives-based oxime esters **1-9**.

For the two-component systems under examination, the co-initiators were first an iodonium salt, specifically *bis*(4-*tert*-butylphenyl)iodonium hexafluorophosphate (hereafter referred to as Iod or Speedcure 938) from Lambson Ltd (UK) and a tertiary amine, ethyl 4-dimethylaminobenzoate (EDB) from Sartomer-Lambson (UK). Trimethylolpropane triacrylate (TMPTA) was sourced from Sartomer (located in Verneuil, France). Notably, these reagents were utilized in their received state, with no further purification. Chemical structures of these compounds are depicted in Scheme 2.

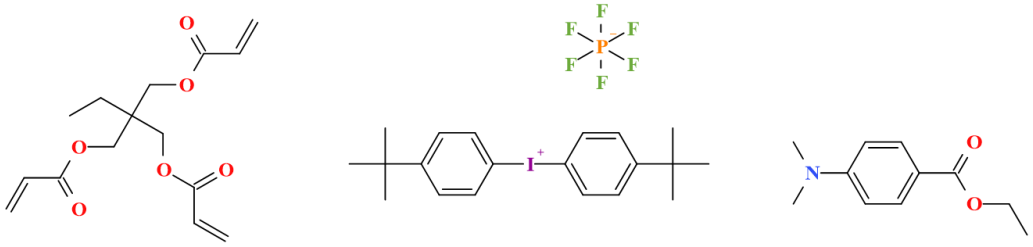

TMPTA **Iod** **EDB**

Scheme 2. Chemical structures of the monomer and the different additives.

2.1 Photopolymerization Experiments

The novel compounds were combined with either Iod or EDB in TMPTA as the monomer to generate photosensitive formulations. For the preparation of thin samples, these formulations were layered between two polypropylene films. For thick sample preparation, the formulations were introduced dropwise into prefabricated molds. Photosensitive formulations were then subjected to light exposure, employing light-emitting diodes (LED) that emit at wavelengths of 365, 385 and 405 nm (I_0 = 110 mW·cm^{-2}) under ambient conditions. Polymerization kinetics were monitored in real-time using Fourier-transform infrared spectroscopy (FTIR, JASCO FTIR 4100). Monitoring of the polymerization process was achieved by targeting the IR peak at approximately 1620 cm^{-1} and 6120 cm^{-1} corresponding to a characteristic peak of TMPTA in thin and thick samples, respectively. Conversion of the acrylate function during a specified irradiation duration was established to determine the polymerization profiles, which is delineated by the following relationship[15,33]:

$$\text{Conversion}(\%) = \frac{A_0 - A_t}{A_0} \times 100$$

where A_0 is the initial peak area before irradiation and A_t is the peak area after irradiation for a given time t.

2.2 UV-Vis Absorption and Steady-State Photolysis

Steady-state photolysis experiments were conducted by UV-visible absorption spectroscopy, employing a JASCO V-730 UV-visible spectrometer. Solutions composed of the new compounds dissolved in dichloromethane were exposed to irradiation in a cuvette at room temperature, utilizing a LED with a wavelength of 405 nm.

2.3 Fluorescence Quenching and Fluorescence Lifetime

Experiments pertaining to fluorescence quenching were carried out utilizing a JASCO FP-6200 spectrometer. Subsequent analyses of the obtained fluorescence quenching spectra enabled the determination of the Stern-Volmer coefficients (K_{sv}) by calculating the slope values as per the Stern-Volmer treatment[34]. Moreover, lifetimes

of the fluorescence-excited states were determined using a HORIBA PPD-850 instrument. Experimental conditions included an excitation wavelength (λ_{exc}) of 367 nm and a pulse duration shorter than 1.4 ns.

2.4 Electron Spin Resonance – Spin Trapping (ESR-ST)

Formulations used for the different tests were prepared with the compounds/Iod or compounds/EDB combinations in *tert*-butylbenzene, with concentrations of 10^{-3} M for Iod, 10^{-3} M for EDB, and 10^{-4} M for PI. Subsequent to ensuring nitrogen saturation, which was achieved at ambient temperature, the solution underwent irradiation using a LED@405 nm. *N*-*tert*-butylbenzonitrone (PBN) served as a spin trap agent at a concentration of 10^{-3} M. An X-band spectrometer (Bruker EMXplus) was employed to detect the formation of free radicals. Following this detection, ESR spectra were simulated using the PES WINSIM software.[34]

2.5 Direct Laser Write

Direct laser write experiments were conducted in a custom-made tank with a thickness of 2 mm. Fabrication of the tridimensional patterns was achieved through irradiation from a computer-controlled 405 nm laser diode. Intensity of the laser impinging the sample surface approximated 110 mW, and the spot size was roughly 50 μm. The writing duration for these patterns was approximately 3 minutes. Following the direct laser writing process, the precise shapes of the different 3D patterns were characterized by a numerical optical microscope (DSX-HRSU, OLYMPUS Corporation). This step allowed for a detailed evaluation of the final patterns produced by this innovative process.

2.6 Computational Procedure

Gaussian 16 suite of programs were used to perform computational chemistry using the UB3LYP/6-31G* level.

3 Results and Discussions

3.1. Synthesis of the Photoinitiators

Synthesis of the nine oxime esters **1-9** was achieved by mean of a multistep synthesis starting from 2,3-diaminonaphthalene-1,4-dione **R1** [35] and 4-(1,3-dioxolan-2-yl)-2,5-*bis*(dodecyloxy)benzaldehyde **R2** [36] as the reagents. Formation of the imidazole cycle could be obtained in DMF, upon heating at 90°C overnight. 2-(4-(1,3-Dioxolan-2-yl)-2,5-*bis*(dodecyloxy)phenyl)-1*H*-naphtho[2,3-*d*]imidazole-4,9-dione **R3** could only be obtained in low yield due to the difficulty to make it precipitate. By treatment in acidic conditions, the acetal group could be hydrolyzed, enabling to get 4-(4,9-dioxo-4,9-dihydro-1*H*-naphtho[2,3-*d*]imidazol-2-yl)-2,5-*bis*(dodecyloxy)benzaldehyde R4 in 91% yield. Noticeably, all attempts to produce **R4** starting from **R1** and **R5** failed. Irrespective of the reaction conditions, 2,2'-(2,5-*bis*(dodecyloxy)-1,4-phenylene)*bis*(1*H*-naphtho[2,3-*d*]imidazole-4,9-dione) **R6** was isolated as the unique product of the reaction (See Scheme 3). Once formed, **R4** was converted as the oxime **R7** using hydroxylamine hydrochloride and sodium acetate as the base in a mixture of water, methanol and THF. Oxime esters **1-9** were prepared with nine different commercially available acid chlorides and triethylamine as the base. The different dyes **1-9** could be obtained with reaction yields ranging between 21 and 70 % yields.

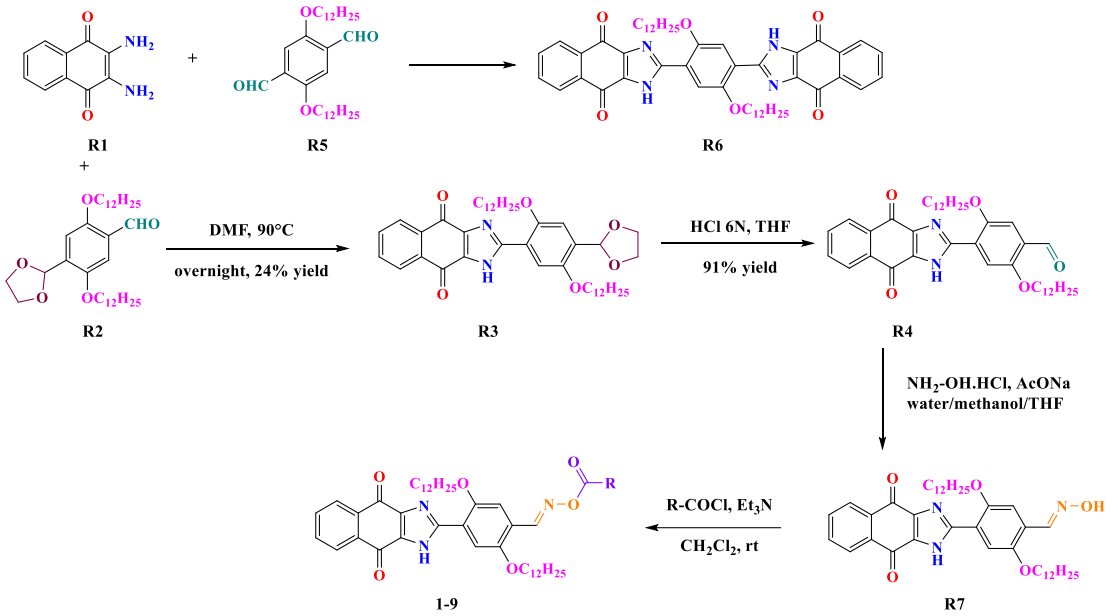

Scheme 3. Synthetic route to oxime esters **1-9**.

3.2. Light Absorption Properties

UV-Vis absorption spectra of the different photoinitiators under investigation are presented in Figure 1 and the spectra were collected in dichloromethane as the solvent. Optical properties of the different oxime esters are summarized in Table 1. The maximum absorption wavelength (λ_{max}) for the nine compounds **1-9** was found to be at ca. 375 nm. Similarity of the absorption maxima is consistent with the chromophore located on the naphthoquinone side. Notably, compounds **3** and **9** exhibited slightly higher molar absorptivity at the maximum absorption wavelength than the other seven oxime esters. Additionally, in the visible range i.e., at $\lambda = 405$ nm, compounds **3**, **8**, and **9** showed superior absorption characteristics than the other dyes. Nonetheless, all the photoinitiators displayed satisfactory absorption properties at 405 nm since molar extinction coefficient higher than 6 000 $M^{-1}.cm^{-1}$ were determined, demonstrating their potential use as photoinitiators at this wavelength.

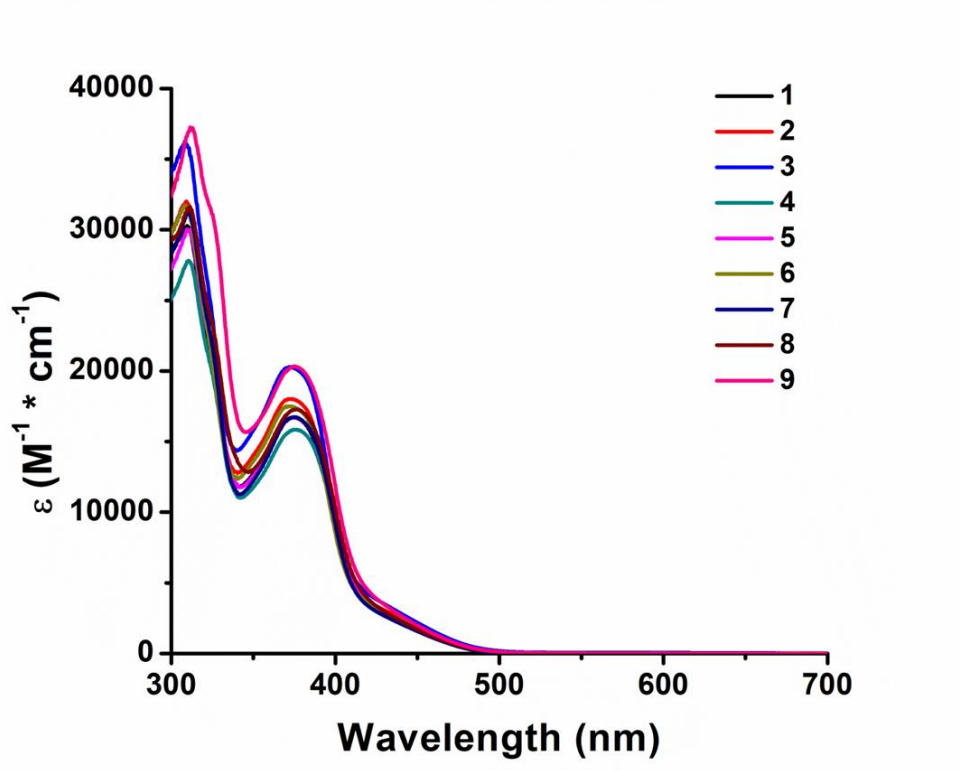

Figure 1. UV-visible absorption spectra of compounds **1-9** in dichloromethane.

Table 1. Light absorption properties of compounds **1-9** in dichloromethane: maximum absorption wavelengths λ_{max}; molar extinction coefficients at λ_{max} (ε_{max}) and molar extinction coefficients at the emission wavelength of the LED@405 nm ($\varepsilon_{@405\ nm}$)

No.	λ_{max} (nm)	ε_{max} ($M^{-1}\cdot cm^{-1}$)	$\varepsilon_{@405\ nm}$ ($M^{-1}\cdot cm^{-1}$)
1	375	16710	6530
2	373	18020	6390
3	372	20280	7190
4	375	15850	6680
5	374	16700	6930
6	372	17510	6200
7	376	16730	6580
8	376	17270	7640
9	375	20320	8800

3.3. Study of new compounds as Type I photoinitiators

In the conducted experiments, the trifunctional acrylic monomer TMPTA was

selected as the polymerizable unit for the different photoinitiating systems which contained a 0.1 wt% (relative to TMPTA) concentration of Type I photoinitiator. This system was then subjected to irradiations with blue LEDs at various irradiation wavelengths (365, 385 and 405 nm). Final conversion rates of the acrylate functional groups in both thin and thick films were measured using Real-Time Fourier-Transform Infrared Spectroscopy (RT-FTIR). The corresponding photopolymerization profiles and acrylate function final conversions (FCs) are presented in Figure 2 and Table 2, respectively.

The nine novel compounds can be distinguished by the substituents attached on the carboxyl side of oxime esters, which resulted in their classification into three different categories: those with methoxymethyl, alkyl, and aryl substituents. As depicted in Figure 2, all compounds could successfully act as Type I photoinitiators when exposed to a LED light at 405 nm. Among the different structures, compound **3** (bearing a pentyl group on the carboxyl side) yielded the highest FC of 85% in thin samples. In thick samples, compound **3** maintained the highest FC of 53%. However, regardless of the FC or the conversion rate, the overall polymerization rate for thick samples was noticeably slower, contributing to significant differences between the monomer conversions obtained in thin and thick films. This discrepancy can be attributed to internal filtering effects, which are well-known to decrease the light transmittance by increasing the optical density, in accordance with the Beer-Lambert law.

Interestingly, the photoinitiation efficiency seemed to favor compounds with either methoxy or alkyl groups on the carboxyl side, as opposed to those with aryl substituents. For instance, compounds **1**, **2**, **3**, and **6** showed superior performance in thick sample, providing faster conversion rates and higher FCs. While the photoinitiation abilities of these compounds were found to correlate with their absorption characteristics to some extent (such as for compound 3), there was no strict relationship between molar extinction coefficient and monomer conversion (as evidenced with compound **9**). To substantiate this observation, further control experiments involving LEDs closer to the

maximum absorption wavelength of the novel compounds were warranted.

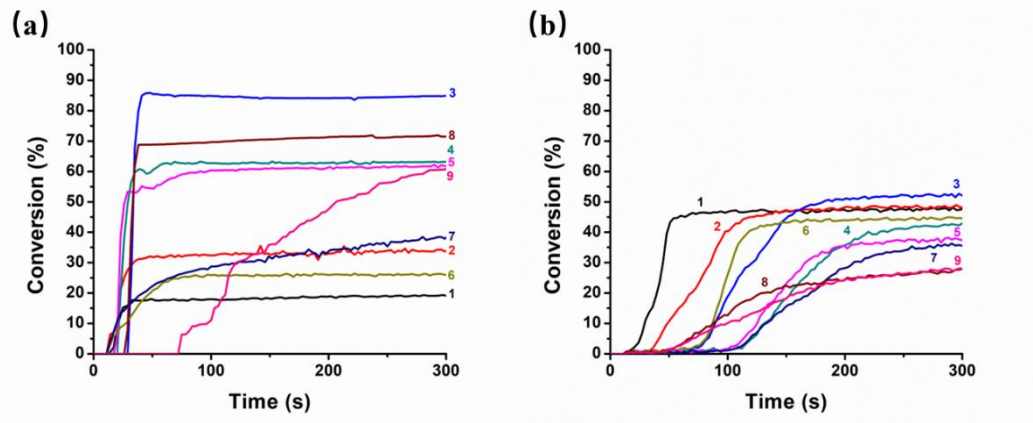

Figure 2. Photopolymerization profiles of acrylate functions (double bond conversion vs irradiation time) upon exposure to a LED@405 nm in the presence of a) compounds (0.1 wt%)/TMPTA in laminate (thickness at ≈ 25 μm); b) compounds (0.1 wt%)/TMPTA under air (thickness at ≈ 1.5 mm). The irradiation starts at t = 10 s.

Table 2. Final acrylate function conversions (FCs) using compounds (0.1 wt%) after 300 s of irradiation with a LED light (λ = 365, 385 and 405 nm).

No.	Thin samples (25 μm) @405 nm	Thick samples (1.5 mm) @405 nm	Thick samples (1.5 mm) @365 nm	Thick samples (1.5 mm) @385 nm
1	20%	49%	15%	43%
2	34%	49%	7%	28%
3	85%	53%	3%	24%
4	63%	44%	1%	5%
5	62%	39%	1%	16%
6	26%	45%	4%	32%
7	39%	38%	1%	9%
8	72%	29%	2%	14%
9	62%	30%	1%	10%

Given that all new compounds exhibit an absorption maximum around 375 nm, LEDs emitting at 365 and 385 nm were utilized under identical experimental conditions.

The same photopolymerization experiments were carried out on thick samples, in order to validate the reactivity of the tested structures at these shorter wavelengths. The FCs are presented in Table 2. As depicted in Figure 3b, at 385 nm, a general reduction of the initiation capability could be determined for most of the new compounds. This was especially true for compounds **2, 3, 6**, with alkyl substituents, and the remaining compounds bearing aryl substituents. Notably, compound **1** could maintain a FC comparable to that achieved at 405 nm, although the photopolymerization rate significantly declined. When the wavelength was further reduced to 365 nm, nearly all new compounds lost their photoinitiating abilities, with the samples failing to effectively polymerize (Figure 3a). Consequently, despite the UV-Vis absorption spectra indicating superior light absorption for the new compounds at 365 and 385 nm compared to 405 nm, a direct correlation between photoinitiating abilities and absorption properties could not be established. Considering these observations, and the fact that the best results were obtained under LED@405nm irradiation—a wavelength commonly employed for both scientific research and commercial applications—this light source was selected for the ongoing investigations of the different structures as Type II photoinitiators or in multicomponent systems.

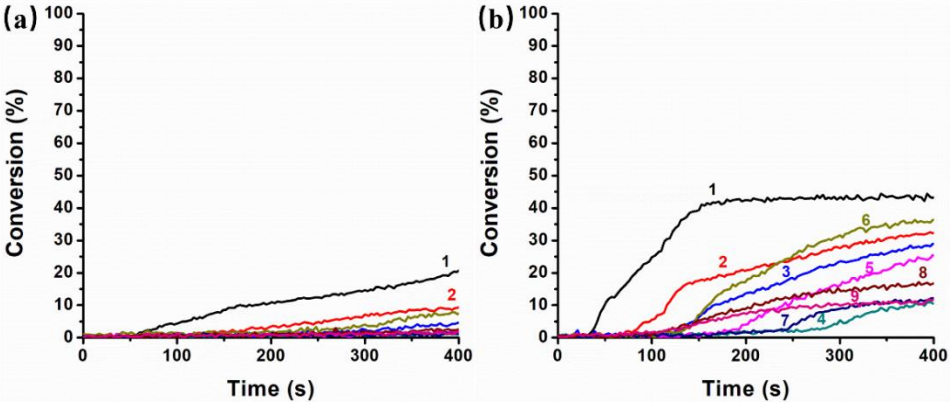

Figure 3. Photopolymerization profiles of acrylate functions (double bond conversion vs irradiation time) using compounds (0.1 wt%)/TMPTA under air (thickness at ≈ 1.5 mm) in the presence of a) upon exposure to a LED@365 nm; b) upon exposure to a LED@385 nm. The irradiation starts at t = 10 s.

To gain a more comprehensive understanding of the compounds' behavior post-irradiation, photolysis experiments were conducted on compounds **1**, **3**, and **9**, which respectively bear methoxymethyl, alkyl, and aryl groups on the carboxyl side. These results are depicted in Figure 4. Photolysis experiments revealed that the three compounds could undergo a photolysis upon irradiation, with each of them exhibiting varying degrees of blue shift of their absorption maxima. By comparing the consumption rate for each sample within a five-minute period (calculated based on the decrease of the absorption peak at the maximum absorption wavelength of 375 nm), compound **3** led to a decrease of the absorption intensity to 21%, followed by compound 1 (16%), and by compound **9** which showed the lowest consumption of 10% (see Figure 4d). This demonstrates that derivatives with alkyl substituents had the fastest photolysis rate in dichloromethane upon irradiation at 405 nm with a LED, followed by those with methoxy groups. Derivatives containing aryl substituents showed the lowest photolysis yield. These photolysis results are in line with the photopolymerization results, indicating that a better photolysis capacity enhances the photoinitiation ability of photoinitiators. This underscores the role of the substituent group on the carboxyl side in influencing the overall performance of these novel photoinitiators.

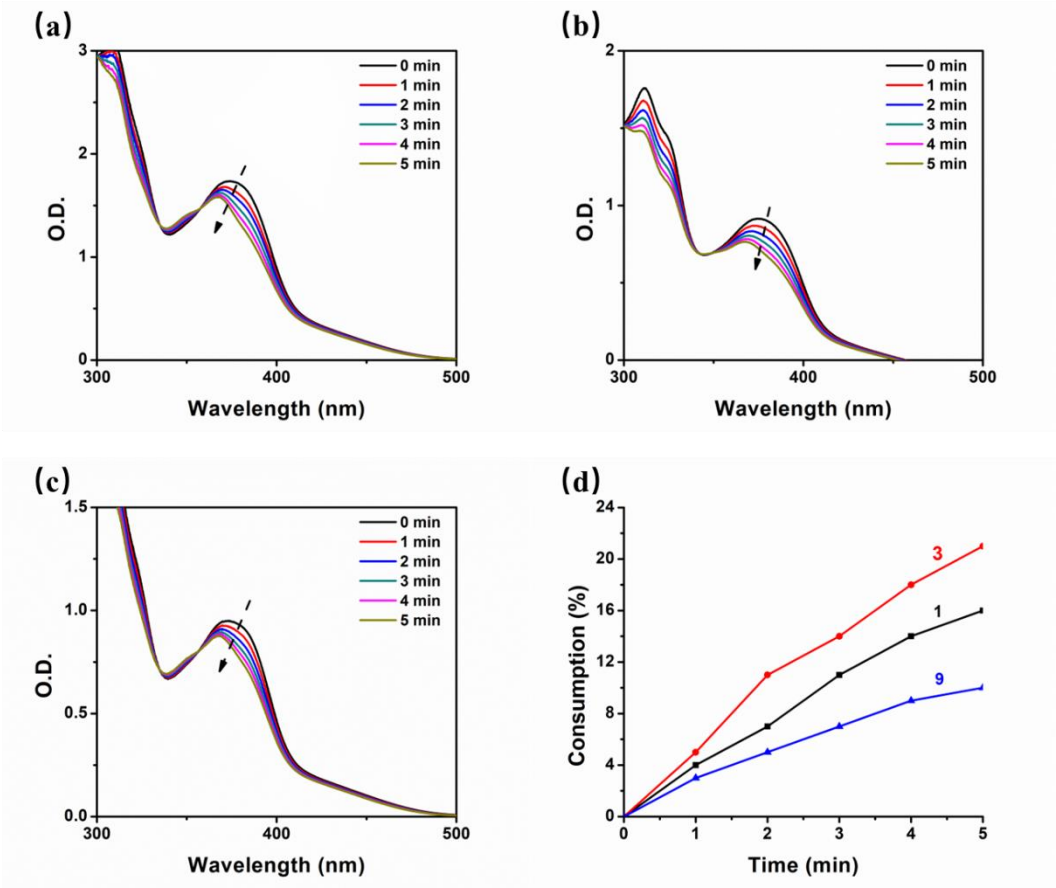

Figure 4. UV-vis absorption spectra of a) compound **1** (5×10^{-5} M), b) compound **3** (5×10^{-5} M) and c) compound **9** (5×10^{-5} M) under air in dichloromethane (LED@405 nm); d) consumption of compounds **1, 3, 9**.

ESR experiments were carried out to discern the specific types of free radicals generated during photopolymerization. It's noteworthy that when compound **1** was irradiated with a LED light at 405 nm for 25 seconds, the ESR signal (a_N = 13.4 G, a_H = 1.8 G) exhibited a significant enhancement (refer to Figure 5). This can be attributed to the adducts formed by the interaction of acyloxy groups and PBN. Formation of these acyloxy radicals stems from the γ-scission of the N-O bond within the oxime ester structure[18]. In theory, this is followed by a decarboxylation process, leading to further fragmentation to generate new free radicals. As indicated in previous studies, not all decarboxylation reactions are necessarily observable[26]. Consistent with this, the current study did not record the generation of CO_2, a common byproduct formed by the decarboxylation reaction and thus during the photopolymerization experiments. This

underscores the complexity and variable nature of such chemical reactions. The successful detection of these radicals provides the confirmation of the proposed photoinitiation mechanism.

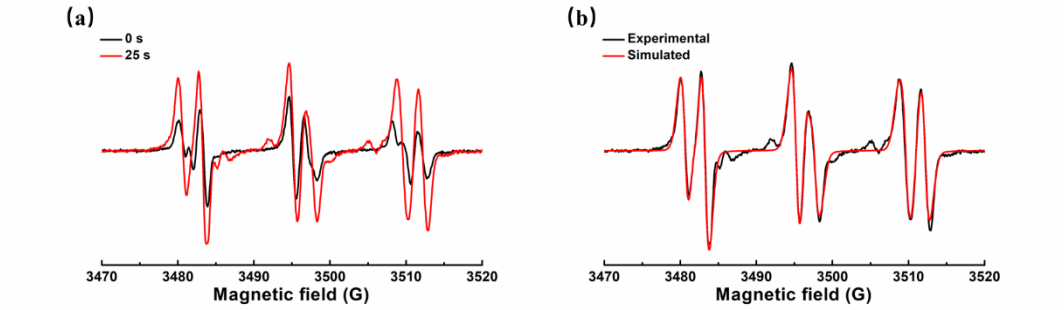

Figure 5. ESR spectra of compound **1** in *tert*-butylbenzene. a) before and after 25 s LED@405 nm irradiation; b) experimental and simulated.

The singlet excited state energy (E_{S1}) was obtained by calculating the intersection of the normalized UV-Vis absorption and fluorescence spectra of the different compounds (see Figures 6a, b, c and Figure S1). Table 3 gives the corresponding N-O bond dissociation energies (BDEs) and excited state properties (singlet and triplet excited state energies) for all compounds. From the calculations, the S_1 dissociation enthalpies of all the compounds are negative, indicating that the N-O cleavage process in this excited state is energetically favorable. However, the T_1 dissociation enthalpies of all compounds except compounds **2**, **5**, **7**, **8**, and **9** are **0** or positive, and the T_1 dissociation enthalpies of compounds **2**, **5**, **7**, **8**, and **9** are also less favorable than their S_1 dissociation enthalpies. So the new compounds are probably more easily cleaved from the singlet state. Simultaneously, the fluorescence lifetimes for compounds **1, 3,** and **9** were measured (refer to Figure 6d, e, f). Compound **9**, bearing an aryl substituent, displayed the longest lifetime of 2.9 ns. In comparison, compound **1**, with a methoxymethyl substituent, and compound **3**, with an alkyl substituent, displayed fluorescence lifetimes of less than 1.4 ns and 2.3 ns respectively. The elongated fluorescence lifetime results in a slower rate of singlet cleavage for compound **9**, contributing to its distinct photophysical properties.

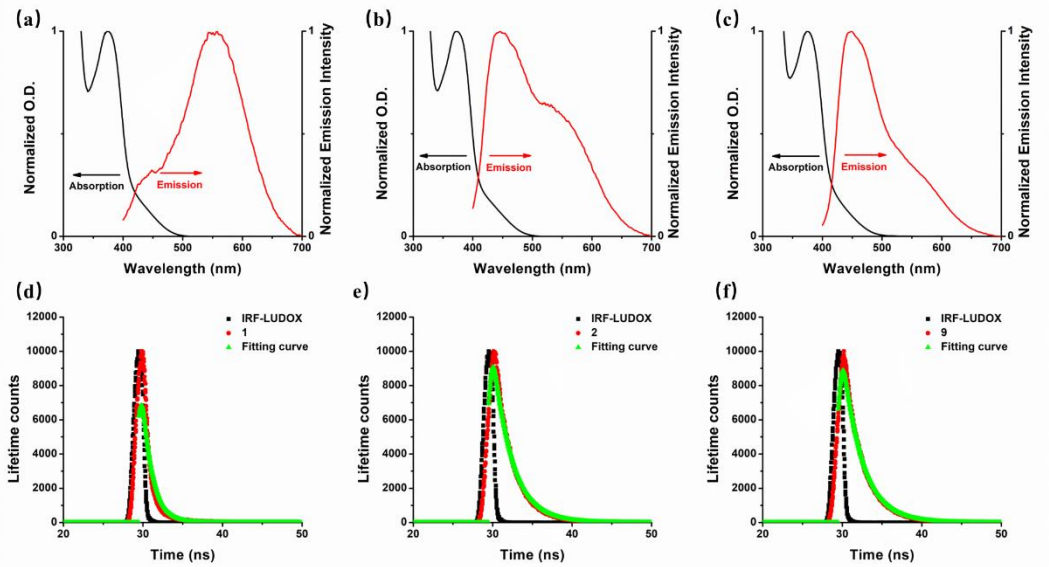

Figure 6. UV-visible absorption and emission spectra of a) compound 1, b) compound 2 and c) compound **9**. Fluorescence lifetimes for d) compound **1**, e) compound **3** and f) compound **9**.

Table 3. Parameters were deduced using molecular modelling techniques. Among them is the bond dissociation energy (BDE) of the N–O bond. The triplet state energy, represented as E_{T1}, was computed, and the enthalpy ($\Delta H_{cleavageT1}$) associated with the cleavage process from this triplet state was determined using the equation $\Delta H_{cleavageT1}$ = BDE - E_{T1}. Additionally, the singlet excited state energy, E_{S1}, was inferred from experimental absorption and fluorescence spectra data. The corresponding enthalpy ($\Delta H_{cleavageS1}$) for the cleavage process from the singlet state was ascertained using the relationship $\Delta H_{cleavageS1}$ = BDE – E_{S1}.

Compound	BDE (kcal/mol)	E_{S1} (kcal/mol)	$\Delta H_{cleavageS1}$ (kcal/mol)	E_{T1} (kcal/mol)	$\Delta H_{cleavageT1}$ (kcal/mol)
1	49.53	66.88	-17.35	48.46	1.07
2	48.08	69.88	-21.8	48.48	-0.4
3	49.19	64.58	-15.39	48.48	0.71
4	48.59	63.19	-14.6	48.48	0.11

5	48.35	63.88	-15.53	48.38	-0.03
6	49.12	61.81	-12.69	48.47	0.65
7	48.11	63.65	-15.54	48.25	-0.14
8	47.22	68.49	-21.27	49.64	-2.42
9	45.74	68.72	-22.98	48.54	-2.8

3.4. Study of new compounds in multicomponent systems

Aiming to broaden the application scope of these novel compounds, two-component photoinitiating systems were designed based on the dye/Iod or dye/EDB configurations. Photopolymerization processes were carried out with the same light source than used in the previous experiments, namely a LED emitting at 405 nm. Figure 7 depicts typical polymerization profiles obtained for thin and thick samples using these two-component systems. Final acrylate functions conversions (FC) obtained with the different two-component systems are summarized in Table 4.

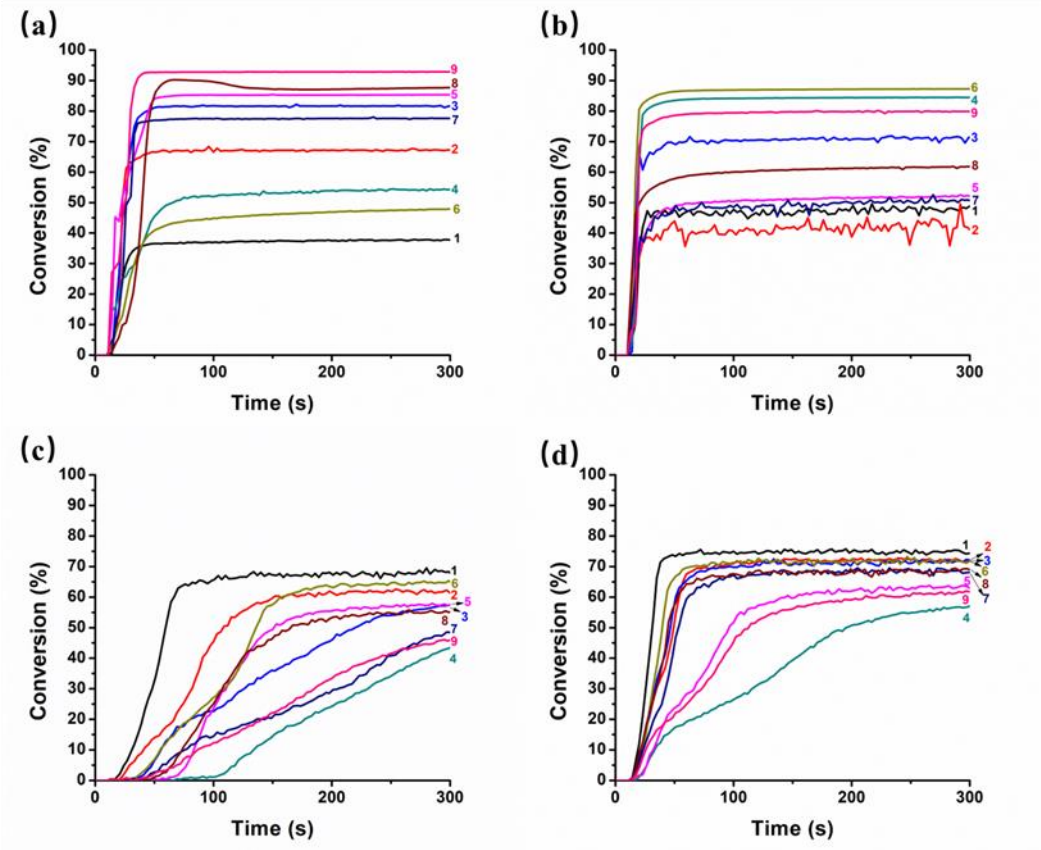

Figure 7. Photopolymerization profiles of acrylate functions (double bond conversion vs irradiation time) upon exposure to a LED@405 nm in the presence of a) compounds

(0.1 wt%)/Iod (2 wt%)/TMPTA in laminate (thickness at ≈ 25 μm); b) compounds (0.1 wt%)/EDB (2 wt%)/TMPTA in laminate (thickness at ≈ 25 μm); b) compounds (0.1 wt%)/Iod (2 wt%)/TMPTA under air (thickness at ≈ 1.5 mm); b) compounds (0.1 wt%)/EDB (2 wt%)/TMPTA under air (thickness at ≈ 1.5 mm). The irradiation starts at t = 10 s.

Table 4. FCs using compounds (0.1 wt%)//Iod (2 wt%) and compounds (0.1 wt%)/EDB (2 wt%) after 300 s of irradiation with a LED@405 nm.

No.	Thin samples (25 μm) in laminate		Thick samples (1.5 mm) under air	
	Compounds/Iod	Compounds/EDB	Compounds/Iod	Compounds/EDB
1	38%	48%	68%	74%
2	67%	40%	61%	72%
3	82%	71%	57%	72%
4	54%	85%	43%	57%
5	85%	52%	57%	63%
6	48%	87%	65%	72%
7	78%	50%	48%	68%
8	88%	62%	56%	69%
9	93%	80%	46%	62%

Remarkably, almost all compounds exhibited a significant improvement of their photoinitiation abilities, regardless of whether the co-initiator was Iod or EDB. The most significant transformation was observed in compound **1**, particularly when applied to the polymerization of thick samples (See Figure 8a). When used as a Type I photoinitiator, compound **1** achieved a FC of 20% when used alone in thin samples, while the FCs rose to 38% with Iod and 48% with EDB. For thick samples, the FC of compound **1** alone was 49%, while adding Iod or EDB raised this to 68% and 74%, respectively. These increased conversion rates led to more rapid polymerizations of the monomer, what was especially notable during the polymerization of thick samples. In the photopolymerization experiments of thin samples, compound **9** exhibited superior performance, achieving a FC of 62% when used alone, 93% when combined with Iod,

and 80% when combined with EDB (Figure 8b). The initiated acrylate conversion rate also displayed an evident increase. This finding demonstrates that all new compounds can form effective two-component photoinitiation systems in combination with Iod or EDB to successfully initiate free radical polymerization. In other words, they all can be employed in multicomponent systems with exceptional photoinitiation properties. Photos of the polymerized samples are shown in Figure S2.

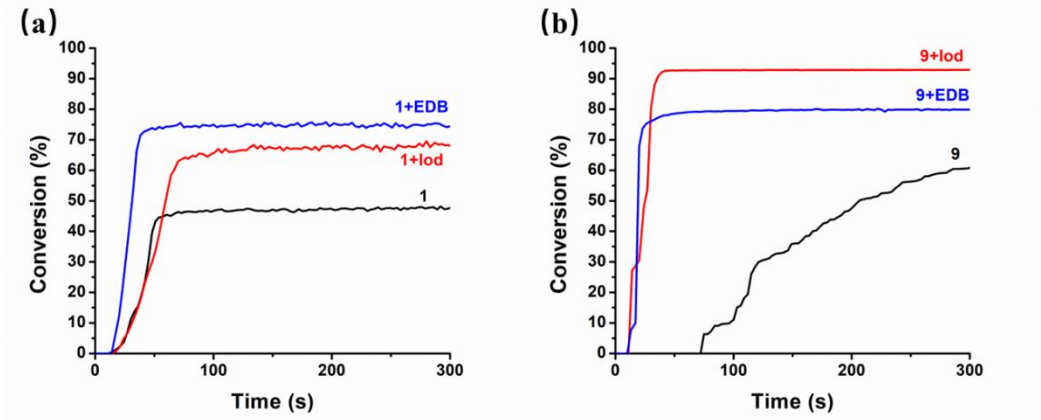

Figure 8. Photopolymerization profiles of acrylate functions (double bond conversion vs irradiation time) upon exposure to a LED@405 nm in the presence of a) compound **1** (0.1 wt%)/TMPTA, compound **1** (0.1 wt%)/Iod (2 wt%)/TMPTA and compound **1** (0.1 wt%)/EDB (2 wt%)/TMPTA under air (thickness at ≈ 1.5 mm); b) compound **9** (0.1 wt%)/TMPTA, compound **9** (0.1 wt%)/Iod (2 wt%)/TMPTA and compound **9** (0.1 wt%)/EDB (2 wt%)/TMPTA in laminate (thickness at ≈ 25 μm). The irradiation starts at t = 10 s.

These findings clearly demonstrate that when an iodonium salt or EDB is incorporated into the photosensitive formulation, the photopolymerization reaction can be efficiently initiated, either by photooxidation or photoreduction processes, when used in conjunction with the new compounds. This process can be ascribed to the following three reactions (Scheme 4): (r1)-(r4). Here, EDB•$_{(-H)}$ and Ar• are considered the principal reactive species. Mechanism (r2) delineates the initiation process characteristic of type I photoinitiators. In contrast, mechanisms (r3) and (r4) describe

the reaction pathways for multicomponent systems. When employing the novel compounds in multicomponent systems, mechanism (r2) competes with either (r3) or (r4).

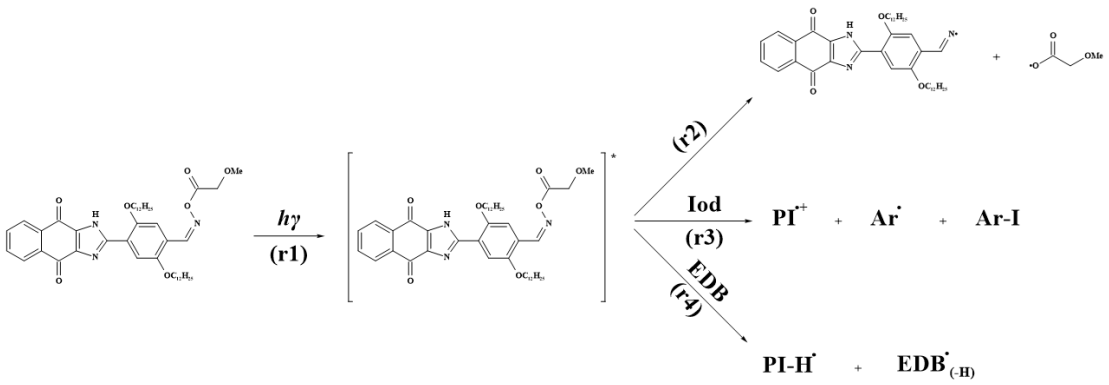

Scheme 4. Proposed photochemical mechanisms.

Figure 9 depicts the steady-state photolysis of compound **1**, compound **1**/Iod, and compound **1**/EDB systems when irradiated with a LED@405nm in dichloromethane. As shown in Figure 9, the ultraviolet absorption peak at 375 nm decreased for each system. When either Iod or EDB is present, the final photolysis percentage is approximately 22%, as compared to 16% when compound **1** is photolyzed independently. The higher photolysis value suggests a successful photochemical interaction of compound 1 with the additive in the excited state, leading to the formation of free radicals EDB•(-H) and Ar•, as discussed earlier. This conclusion is further corroborated by concurrent ESR spin trapping experiments for the compound **1**/Iod and compound **1**/EDB systems, illustrated in Figure 10. For the compound **1**/Iod system, the signal for PBN/Ar• (a_N=14.4G, a_H=2.5G) was successfully captured (See Figure 10a). Likewise, for the compound 1/EDB system, the signal indicating the hyperfine coupling constants for nitrogen and hydrogen (a_N=14.4G, a_H=2.5G) was successfully recorded (Figure 10b), evidencing the generation of an aminoalkyl radical.

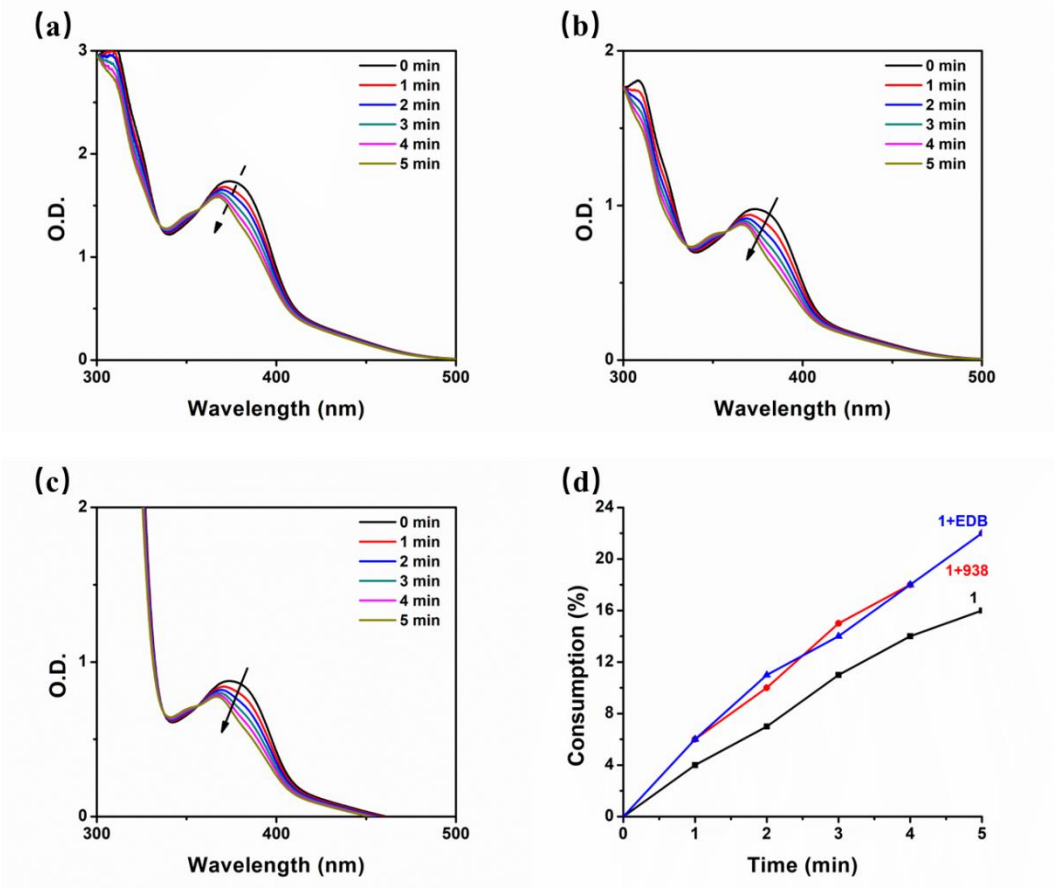

Figure 9. UV-vis absorption spectra of a) compound **1** (5×10^{-5} M), b) compound **1** (5×10^{-5} M)/Iod (10^{-4} M) and c) compound **1** (5×10^{-5} M)/EDB (10^{-4} M) under air in dichloromethane (LED@405 nm); d) consumption of photoinitiating systems.

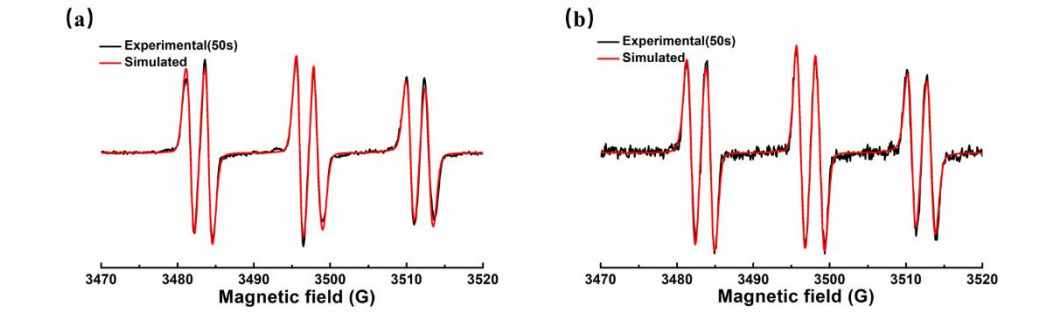

Figure 10. ESR spectra of compound **1**-based photoinitiating systems in *tert*-butylbenzene after 50 s LED@405 nm irradiation. a) compound **1**/Iod; b) compound **1**/EDB.

Fluorescence quenching experiments were performed on compound **1** in acetonitrile to gain deeper insights into its interactions with Iod or EDB, as depicted in

Figure 11. Fluorescence spectra were acquired by progressively increasing the concentration of either EDB or Iod. The quantum yield ($\varphi_{quenching}$) was calculated in accordance with the Stern-Volmer equation:

$$\varphi_{quenching} = \frac{K_{sv} \cdot C}{1 + K_{sv} \cdot C}$$

The K_{sv} in the equation represents the Stern–Volmer quenching constant, and c represents the concentration of the quencher. Results of the fluorescence quenching experiments revealed a quantum yield of 21% for compound **1** when Iod was added, whereas this value was of 36% when EDB was introduced. This provides substantial evidence that the interaction between compound **1** and EDB is stronger, leading to a faster polymerization rate and a higher FC during the free radical photopolymerization of thick samples using the compound **1**/EDB system.

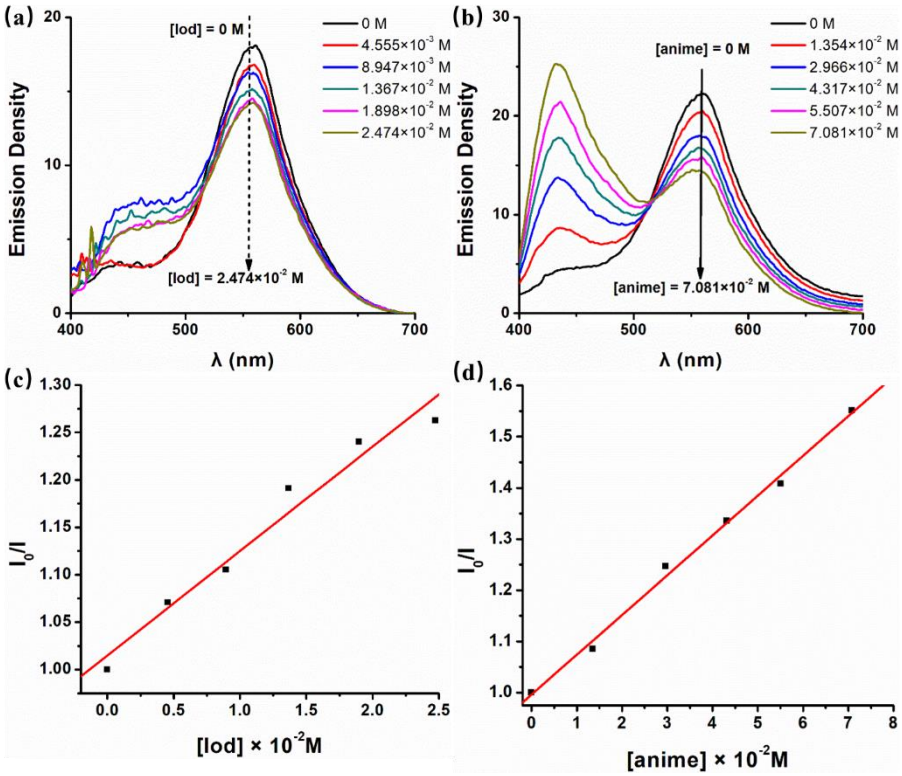

Figure 11. Fluorescence quenching of a) compound **1** (5×10^{-5} M in dichloromethane)/Iod and b) compound **1** (5×10^{-5} M in dichloromethane)/EDB. The Stern–Volmer treatment for c) compound **1**/Iod and d) compound 1/EDB.

The newly developed photoinitiation systems, compound **9**/Iod and compound 9/EDB, were employed for Direct Laser Write for radical photopolymerization of TMPTA, as shown in Figure 12. The resultant 3D printed patterns displayed sharp outlines when observed under a 3D laser scanning microscope. Even though the two-component compound **9**/Iod and compound **9**/EDB systems were not the most impressive photoinitiating systems during the photopolymerization of thick samples, the Direct Laser Write experiments carried out with these systems yielded products that were well-defined and structurally consistent. These observations indicate that the novel compounds can effectively serve in multicomponent systems.

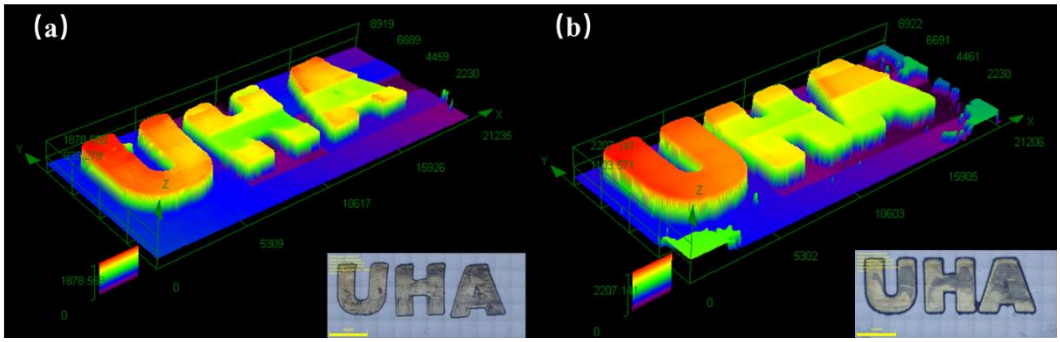

Figure 12. Direct Laser Write (DLW) experiments were conducted using TMPTA. The characterization of the 3D color patterns was executed via numerical optical microscopy. Observations were made in the presence of a) compound **9**/Iod and b) compound **9**/EDB.

4 Conclusion

This study successfully designed and synthesized nine new naphthoquinone-imidazolyl derivatives-based oxime esters, all of them showing intriguing photophysical and photochemical properties. These new compounds can serve both as monocomponent photoinitiators and as part of two-component photoinitiation systems when combined with Iod or EDB. This versatility allows them to operate both as type I photoinitiators and multicomponent systems, achieving a high photopolymerization conversion rate. Addition of co-initiators considerably enhances the performance of the photoinitiation system. The naphthoquinone derivatives were also successfully utilized

in 3D printing experiments, demonstrating their practical applicability.

Acknowledgments

This work was performed using HPC resources of the Mesocentre of the University of Strasbourg and the HPC resources from GENCI-IDRIS (Grant 2023-AD010812313R2 /Jean_Zay). This research project was supported by China Scholarship Council (CSC) (No. 202007030005). P.X. acknowledged funding from the Australian Research Council (FT170100301). This research was funded by the Agence Nationale de la Recherche (ANR) through the PhD grant of Nicolas Giacoletto (ANR-19-CE07-0042, NO PEROX project)

References

1. Andjela, L.; Abdurahmanovich, V.M.; Vladimirovna, S.N.; Mikhailovna, G.I.; Yurievich, D.D.; Alekseevna, M.Y. A review on Vat Photopolymerization 3D-printing processes for dental application. *Dental Materials* **2022**, *38*, e284-e296, doi:https://doi.org/10.1016/j.dental.2022.09.005.
2. Borjigin, T.; Schmitt, M.; Morlet-Savary, F.; Xiao, P.; Lalevée, J. Low-Cost and Recyclable Photocatalysts: Metal Oxide/Polymer Composites Applied in the Catalytic Breakdown of Dyes. *Photochem* **2022**, *2*, 733-751, doi:10.3390/photochem2030047.
3. Xiao, P.; Zhang, J.; Dumur, F.; Tehfe, M.A.; Morlet-Savary, F.; Graff, B.; Gigmes, D.; Fouassier, J.P.; Lalevée, J. Visible light sensitive photoinitiating systems: Recent progress in cationic and radical photopolymerization reactions under soft conditions. *Progress in Polymer Science* **2015**, *41*, 32-66, doi:https://doi.org/10.1016/j.progpolymsci.2014.09.001.
4. Tehfe, M.A.; Louradour, F.; Lalevée, J.; Fouassier, J.-P. Photopolymerization Reactions: On the Way to a Green and Sustainable Chemistry. *Applied Sciences* **2013**, *3*, 490-514, doi:10.3390/app3020490.
5. Lalevée, J.; Morlet-Savary, F.; Dietlin, C.; Graff, B.; Fouassier, J.-P. Photochemistry and Radical Chemistry under Low Intensity Visible Light Sources: Application to Photopolymerization Reactions. *Molecules* **2014**, *19*, 15026-15041, doi:10.3390/molecules190915026.
6. Müller, S.M.; Schlögl, S.; Wiesner, T.; Haas, M.; Griesser, T. Recent Advances in Type I Photoinitiators for Visible Light Induced Photopolymerization. *ChemPhotoChem* **2022**, *6*, e202200091, doi:https://doi.org/10.1002/cptc.202200091.
7. Dietlin, C.; Trinh, T.T.; Schweizer, S.; Graff, B.; Morlet-Savary, F.; Noirot, P.-A.; Lalevée, J. New Phosphine Oxides as High Performance Near- UV Type I Photoinitiators of Radical Polymerization. *Molecules* **2020**, *25*, doi:10.3390/molecules25071671.
8. Liu, S.; Giacoletto, N.; Graff, B.; Morlet-Savary, F.; Nechab, M.; Xiao, P.; Dumur, F.; Lalevée, J. N-naphthalimide ester derivatives as Type I photoinitiators for LED photopolymerization. *Materials Today Chemistry* **2022**, *26*, 101137, doi:https://doi.org/10.1016/j.mtchem.2022.101137.
9. Yu, J.; Gao, Y.; Jiang, S.; Sun, F. Naphthalimide Aryl Sulfide Derivative Norrish Type I Photoinitiators with Excellent Stability to Sunlight under Near-UV LED. *Macromolecules* **2019**, *52*, 1707-1717, doi:10.1021/acs.macromol.8b02309.
10. Borjigin, T.; Noirbent, G.; Gigmes, D.; Xiao, P.; Dumur, F.; Lalevée, J. The new LED-Sensitive photoinitiators of Polymerization: Copper complexes in free radical and cationic photoinitiating systems and application in 3D printing. *European Polymer Journal* **2022**, *162*, 110885, doi:https://doi.org/10.1016/j.eurpolymj.2021.110885.
11. Dumur, F. Recent advances on pyrene-based photoinitiators of polymerization. *European Polymer Journal* **2020**, *126*, 109564, doi:https://doi.org/10.1016/j.eurpolymj.2020.109564.
12. Zhou, J.; Allonas, X.; Ibrahim, A.; Liu, X. Progress in the development of polymeric and multifunctional photoinitiators. *Progress in Polymer Science* **2019**, *99*, 101165, doi:https://doi.org/10.1016/j.progpolymsci.2019.101165.
13. Dumur, F. Recent advances on visible light Phenothiazine-based photoinitiators of

polymerization. *European Polymer Journal* **2022**, *165*, 110999, doi:https://doi.org/10.1016/j.eurpolymj.2022.110999.
14. Jandt, K.D.; Mills, R.W. A brief history of LED photopolymerization. *Dental Materials* **2013**, *29*, 605-617, doi:https://doi.org/10.1016/j.dental.2013.02.003.
15. Dietlin, C.; Schweizer, S.; Xiao, P.; Zhang, J.; Morlet-Savary, F.; Graff, B.; Fouassier, J.-P.; Lalevée, J. Photopolymerization upon LEDs: new photoinitiating systems and strategies. *Polymer Chemistry* **2015**, *6*, 3895-3912, doi:10.1039/C5PY00258C.
16. Liu, S.; Borjigin, T.; Schmitt, M.; Morlet-Savary, F.; Xiao, P.; Lalevée, J. High-Performance Photoinitiating Systems for LED-Induced Photopolymerization. *Polymers* **2023**, *15*, doi:10.3390/polym15020342.
17. Oliveira, D.; Rocha, M.G. Dental Light-Curing—Assessing the Blue-Light Hazard. *Dental Clinics* **2022**, *66*, 537-550.
18. Hammoud, F.; Pavlou, A.; Petropoulos, A.; Graff, B.; Siskos, M.G.; Hijazi, A.; Morlet-Savary, F.; Dumur, F.; Lalevée, J. Naphthoquinone-based imidazolyl esters as blue-light-sensitive Type I photoinitiators. *Polymer Chemistry* **2022**, *13*, 4817-4831, doi:10.1039/D2PY00753C.
19. Borjigin, T.; Schmitt, M.; Giacoletto, N.; Rico, A.; Bidotti, H.; Nechab, M.; Zhang, Y.; Graff, B.; Morlet-Savary, F.; Xiao, P.; et al. The Blue-LED-Sensitive Naphthoquinone-Imidazolyl Derivatives as Type II Photoinitiators of Free Radical Photopolymerization. *Advanced Materials Interfaces* **2023**, *10*, 2202352, doi:https://doi.org/10.1002/admi.202202352.
20. Peng, X.; Zhu, D.; Xiao, P. Naphthoquinone derivatives: Naturally derived molecules as blue-light-sensitive photoinitiators of photopolymerization. *European Polymer Journal* **2020**, *127*, 109569, doi:https://doi.org/10.1016/j.eurpolymj.2020.109569.
21. Dumur, F. Recent advances on naphthoquinone-based photoinitiators of polymerization. *European Polymer Journal* **2023**, *193*, 112120, doi:https://doi.org/10.1016/j.eurpolymj.2023.112120.
22. Symons, P. Quinones for redox flow batteries. *Current Opinion in Electrochemistry* **2021**, *29*, 100759, doi:https://doi.org/10.1016/j.coelec.2021.100759.
23. Begantsova, Y.E.; Zvagelsky, R.; Baranov, E.V.; Chubich, D.A.; Chechet, Y.V.; Kolymagin, D.A.; Pisarenko, A.V.; Vitukhnovsky, A.G.; Chesnokov, S.A. Imidazole-containing photoinitiators for fabrication of sub-micron structures by 3D two-photon polymerization. *European Polymer Journal* **2021**, *145*, 110209, doi:https://doi.org/10.1016/j.eurpolymj.2020.110209.
24. Allonas, X.; Obeid, H.; Fouassier, J.-P.; Kaji, M.; Ichihashi, Y.; Murakami, Y. Photochemistry and polymerization efficiency of bis-imidazole based photoinitiator systems. *Journal of Photopolymer Science and Technology* **2003**, *16*, 123-128.
25. Dey, N.; Kulhánek, J.; Bureš, F.; Bhattacharya, S. Imidazole-Functionalized Y-Shaped Push–Pull Dye for Nerve Agent Sensing as well as a Catalyst for Their Detoxification. *The Journal of Organic Chemistry* **2021**, *86*, 14663-14671, doi:10.1021/acs.joc.1c01488.
26. Liu, S.; Giacoletto, N.; Schmitt, M.; Nechab, M.; Graff, B.; Morlet-Savary, F.; Xiao, P.; Dumur, F.; Lalevée, J. Effect of Decarboxylation on the Photoinitiation Behavior of Nitrocarbazole-Based Oxime Esters. *Macromolecules* **2022**, *55*, 2475-2485, doi:10.1021/acs.macromol.2c00294.
27. Liu, Z.; Dumur, F. Recent advances on visible light Coumarin-based oxime esters as initiators of polymerization. *European Polymer Journal* **2022**, *177*, 111449, doi:https://doi.org/10.1016/j.eurpolymj.2022.111449.

28. Dumur, F. Recent advances on carbazole-based oxime esters as photoinitiators of polymerization. *European Polymer Journal* **2022**, *175*, 111330, doi:https://doi.org/10.1016/j.eurpolymj.2022.111330.
29. Xu, J.; Ma, G.; Wang, K.; Gu, J.; Jiang, S.; Nie, J. Synthesis and photopolymerization kinetics of oxime ester photoinitiators. *Journal of Applied Polymer Science* **2012**, *123*, 725-731, doi:https://doi.org/10.1002/app.34551.
30. Liu, S.; Graff, B.; Xiao, P.; Dumur, F.; Lalevée, J. Nitro-Carbazole Based Oxime Esters as Dual Photo/Thermal Initiators for 3D Printing and Composite Preparation. *Macromolecular Rapid Communications* **2021**, *42*, 2100207, doi:https://doi.org/10.1002/marc.202100207.
31. Zhou, R.; Pan, H.; Wan, D.; Malval, J.-P.; Jin, M. Bicarbazole-based oxime esters as novel efficient photoinitiators for photopolymerization under UV-Vis LEDs. *Progress in Organic Coatings* **2021**, *157*, 106306, doi:https://doi.org/10.1016/j.porgcoat.2021.106306.
32. Qiu, W.; Zhu, J.; Dietliker, K.; Li, Z. Polymerizable Oxime Esters: An Efficient Photoinitiator with Low Migration Ability for 3D Printing to Fabricate Luminescent Devices. *ChemPhotoChem* **2020**, *4*, 5296-5303, doi:https://doi.org/10.1002/cptc.202000146.
33. Schmitt, M. Synthesis and testing of ZnO nanoparticles for photo-initiation: experimental observation of two different non-migration initiators for bulk polymerization. *Nanoscale* **2015**, *7*, 9532-9544, doi:10.1039/C5NR00850F.
34. Lalevée, J.; Blanchard, N.; Tehfe, M.-A.; Morlet-Savary, F.; Fouassier, J.P. Green Bulb Light Source Induced Epoxy Cationic Polymerization under Air Using Tris(2,2 ' -bipyridine)ruthenium(II) and Silyl Radicals. *Macromolecules* **2010**, *43*, 10191-10195, doi:10.1021/ma1023318.
35. Chen, Z.; Wang, J.; Cai, T.; Hu, Z.; Chu, J.; Wang, F.; Gan, X.; Song, Z. Constructing Extended π-Conjugated Molecules with o-Quinone Groups as High-Energy Organic Cathode Materials. *ACS Applied Materials & Interfaces* **2022**, *14*, 27994-28003, doi:10.1021/acsami.2c06252.
36. Kim, H.; Chang, J.Y. Reversible Thermochromic Polymer Film Embedded with Fluorescent Organogel Nanofibers. *Langmuir* **2014**, *30*, 13673-13679, doi:10.1021/la502932x.

TOC graphic:

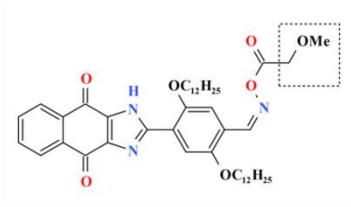

Naphthoquinone-based Oxime Esters

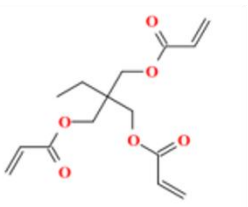

Photocurable Resin (TMPTA)

LED@405nm

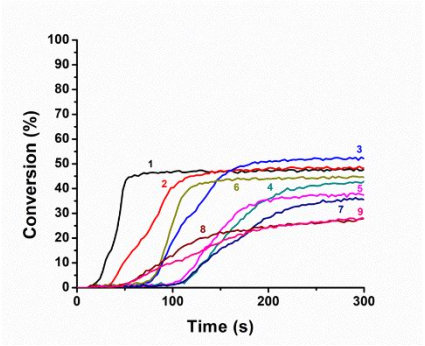

Type I vs. Type II